

ADVANCED ENERGY MATERIALS

Supporting Information

for *Adv. Energy Mater.*, DOI: 10.1002/aenm.201701663

Unravelling Degradation Pathways of Oxide-Supported Pt
Fuel Cell Nanocatalysts under In Situ Operating Conditions

*Henrike Schmies, Arno Bergmann, Jakub Drnec, Guanxiong Wang, Detre Teschner, Stefanie Kühn, Daniel J. S. Sandbeck, Serhiy Cherevko, Martin Gocyla, Meital Shviro, Marc Heggen, Vijay Ramani, Rafal E. Dunin-Borkowski, Karl J. J. Mayrhofer, and Peter Strasser**

Supporting Information

**Unravelling Degradation Pathways of Oxide-supported Pt Fuel Cell Nanocatalysts
under *in situ* Operating Conditions**

*Henrike Schmies¹, Arno Bergmann¹, Jakub Drnec², Guanxiong Wang³, Detre Teschner^{4,5},
Stefanie Kühl¹, Daniel J. S. Sandbeck⁶, Serhiy Cherevko⁶, Martin Gocyla⁷, Meital Shviro⁷,
Marc Heggen⁷, Vijay Ramani³, Rafal E. Dunin-Borkowski⁷, Karl J.J. Mayrhofer⁶, Peter
Strasser^{1*}*

¹ Department of Chemistry, Chemical Engineering Division, Technical University of Berlin, 10623
Berlin, Germany

² European Synchrotron Radiation Facility (ESRF), 38000 Grenoble, France

³ School of Engineering & Applied Science, Washington University in St. Louis, 63130 St. Louis, USA

⁴ Department of Heterogeneous Reactions, Max-Planck-Institute for Chemical Energy Conversion,
45470 Mühlheim an der Ruhr, Germany

⁵ Department of Inorganic Chemistry, Fritz-Haber-Institut der Max-Planck-Gesellschaft, 14195 Berlin,
Germany

⁶ Helmholtz-Institute Erlangen-Nürnberg for Renewable Energy (IEK-11), Forschungszentrum Jülich,
91058 Erlangen, Germany

⁷ Ernst-Ruska Centre for Microscopy and Spectroscopy with Electrons and Peter Grünberg Institute,
Forschungszentrum Jülich, 52425 Jülich, Germany

*Email: pstrasser@tu-berlin.de

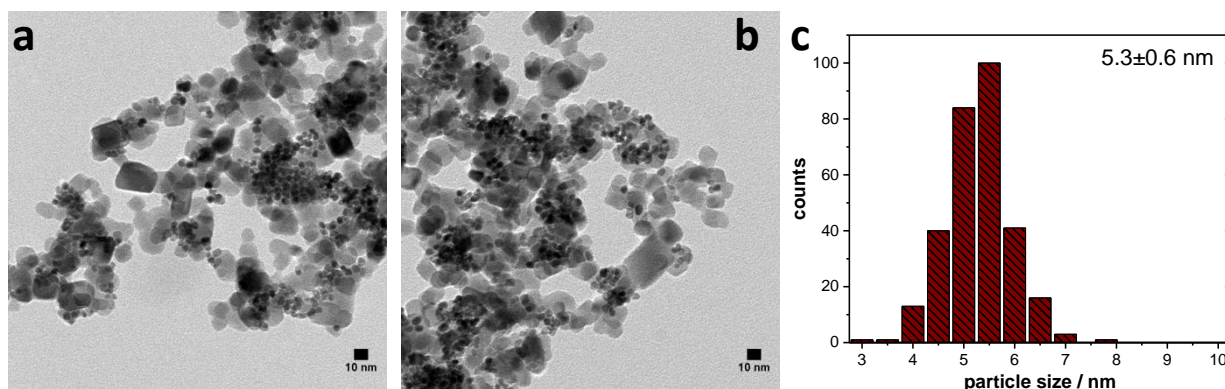


Figure S1. TEM images of as prepared Pt nanoparticles on the ITO support which was used for the HP-AST experiments with a weight loading of 29.9 wt% (a,b) and the corresponding histogram showing particle size distribution (c). Histograms were obtained by measuring the diameter of at least 200 particles with errors obtained from standard deviation of mean particle diameter.

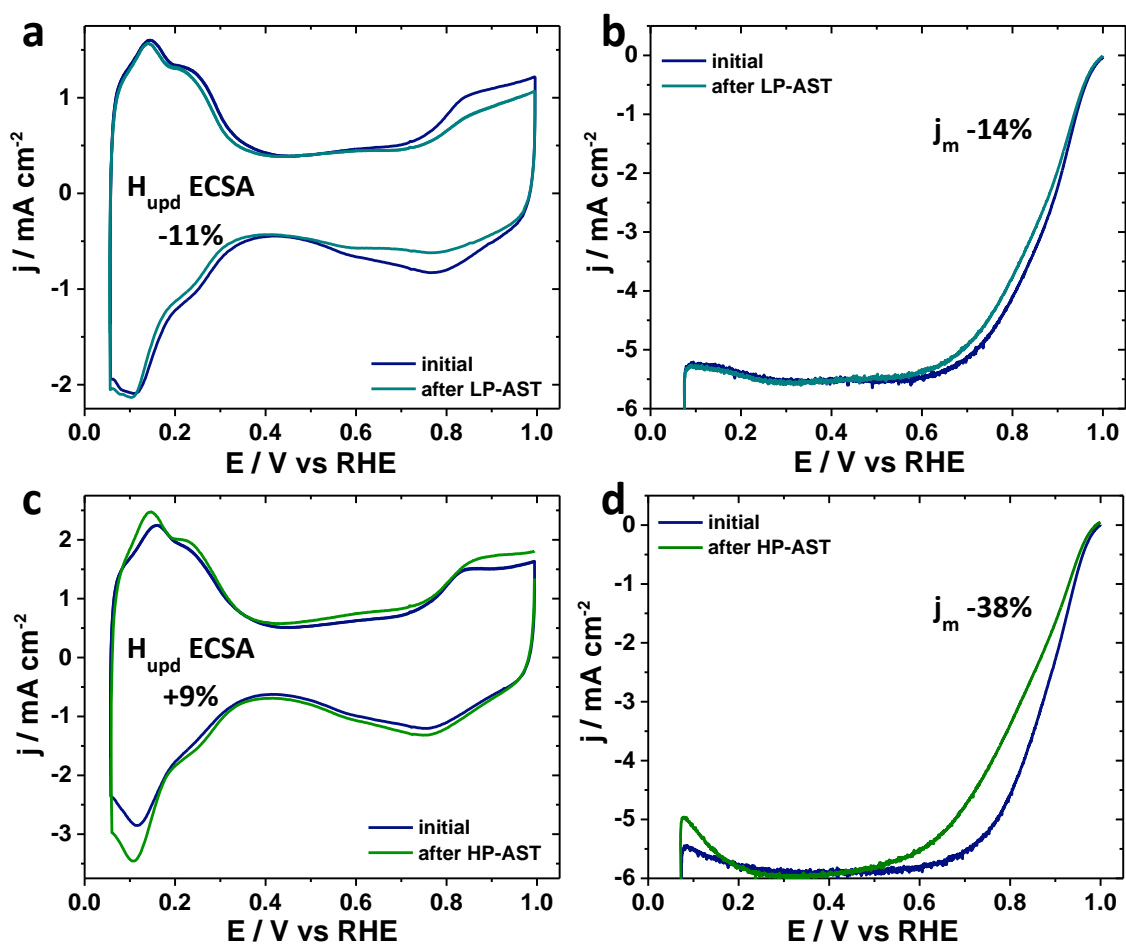


Figure S2. Cyclic voltammograms of Pt/C reference catalyst (weight loading 20 wt% Pt on carbon) before and after potential cycling in lower (a) and higher (c) potential region. CVs were recorded in nitrogen saturated electrolyte from 0.05-1 V with a scan rate of 100 mV s⁻¹. Figure b and d are showing

LSVs of the particular states LSVs were recorded in oxygen saturated electrolyte from 0.05-1 V with a scan rate of $5 \text{ mV}\cdot\text{s}^{-1}$ and 1600 rpm. All electrode potentials have been corrected for iR drop.

Table S1. Comparison of j_m and ECSA before and after LP- and HP-AST for Pt/C reference catalyst. j_m was determined at 0.9 V. ECSAs were determined by integrating the H-desorption and adsorption area between 0.05-0.4 V and subtracting the capacitive current.

	LP-AST		HP-AST	
	initial	after	initial	after
$j_m / \text{A mg}_{\text{Pt}}^{-1}$	0.18	0.15	0.16	0.10
$\text{ECSA} / \text{m}^2 \text{g}_{\text{Pt}}^{-1}$	61.1	54.0	61.4	67.0

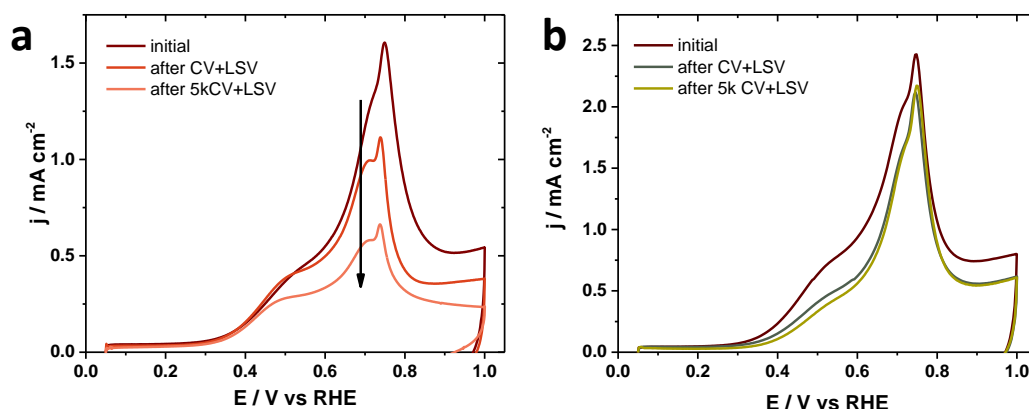


Figure S3. Electrochemical CO stripping experiments for Pt/ITO electrocatalyst. For the two different stability tests in low (a) and high (b) potential regime three different points in the characterization protocol were chosen for CO stripping: initial, after CV+LSV and after 5k CV+LSV.

Table S2. Comparison of ECSAs based on the integration in the H_{upd} and the CO oxidation potential range for Pt/ITO. CO-ECSAs were determined by integrating the CO oxidation peak area from the first cycle of the CO stripping experiment after subtraction of the second cycle representing the bare CO-free surface. H_{upd} -ECSAs were determined by subtracting the first from the second cycle of the CO stripping experiment.

$\text{ECSA} / \text{m}^2 \text{g}_{\text{Pt}}^{-1}$	LP-AST		HP-AST	
	before	after	before	after
CO	25.6	18.4	28.9	27.4
H_{upd}	18.6	17.0	19.3	26.1
CO/H_{upd}	1.38	1.04	1.50	1.05

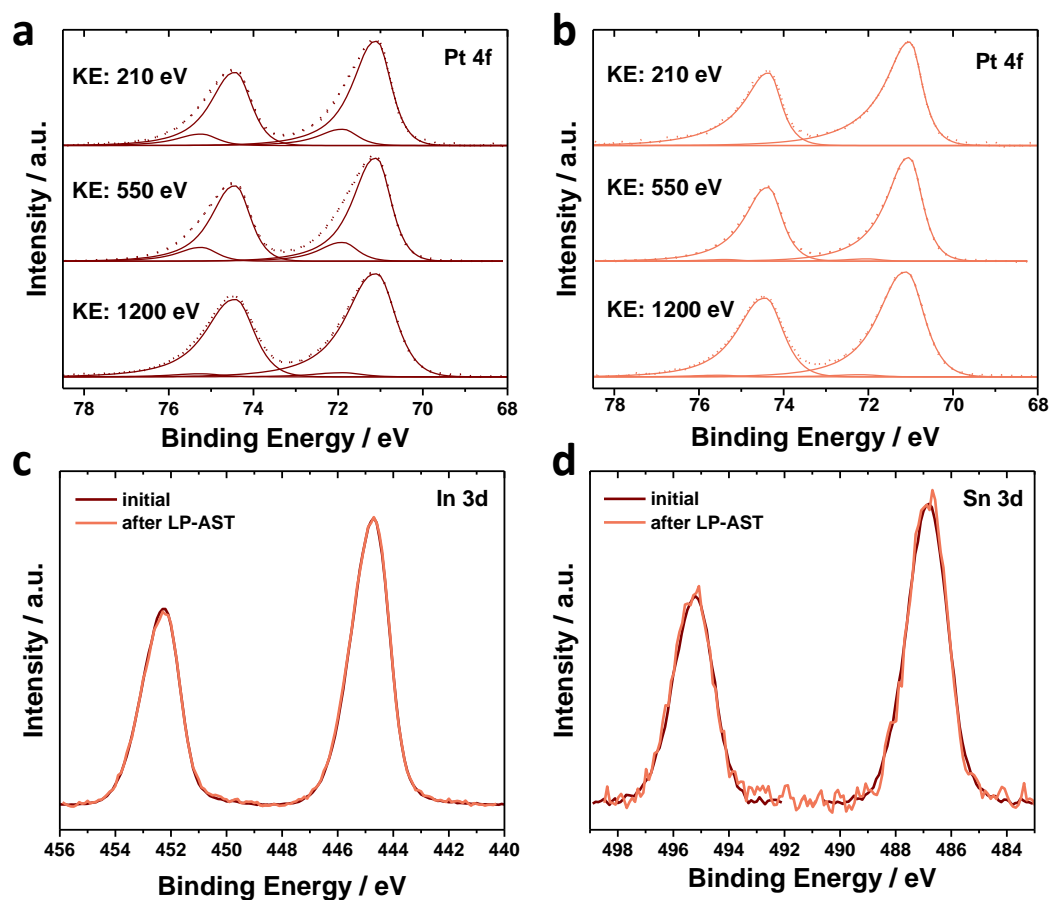


Figure S4. X-ray photoelectron spectroscopy measurements of Pt/ITO. (a) and (b) are showing the Pt 4f depth profiling accessed by the kinetic energy of the photoelectrons of 210, 550 and 1200 eV at the initial (a) and the state after LP-AST (b). Dotted lines represent measured data and solid lines the fits and component peaks. (c) and (d) are showing the 3d core levels for In and Sn, respectively, each at the initial and the cycled state.

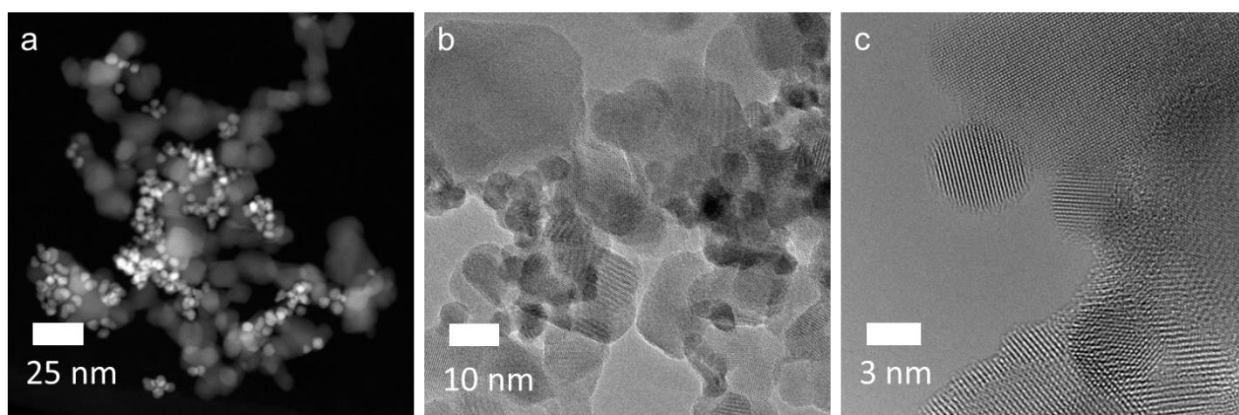


Figure S5. Images of Pt/ITO in the initial state: (a) showing overview HAADF-STEM image, (b) TEM and (c) HR-TEM images.

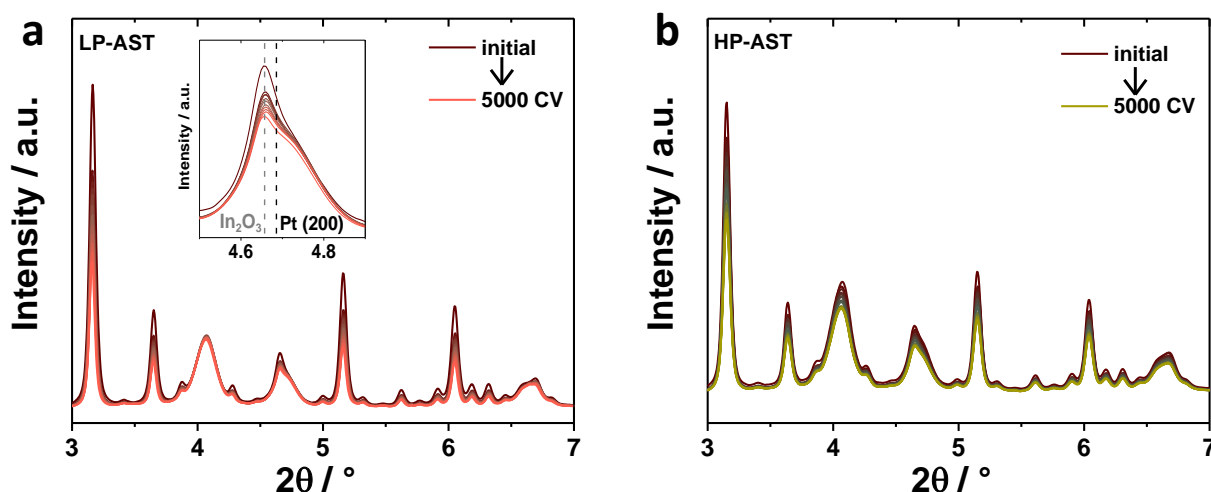


Figure S6. *In situ* HE XRD measurements depicted as the evolution of diffraction patterns from the initial state to the end of the electrochemical cycling for the LP-AST (a) and the HP-AST (b). The inset in (a) is showing the Pt (200) diffraction peak superimposed by an In_2O_3 peak (denoted with dashed vertical lines).

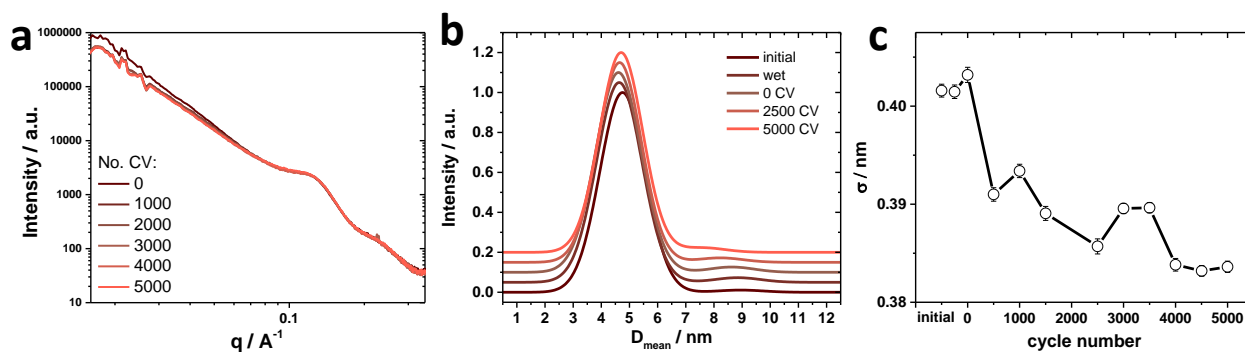


Figure S7. *In situ* ASAXS measurements for LP-AST: background subtracted, Pt element specific scattering curves for selected cycle numbers (a), particle size distribution (PSD) as a function of rel. intensity over the mean particle diameter for selected cycle numbers (b) and the evolution of polydispersity as a function of σ over the cycle number (c).

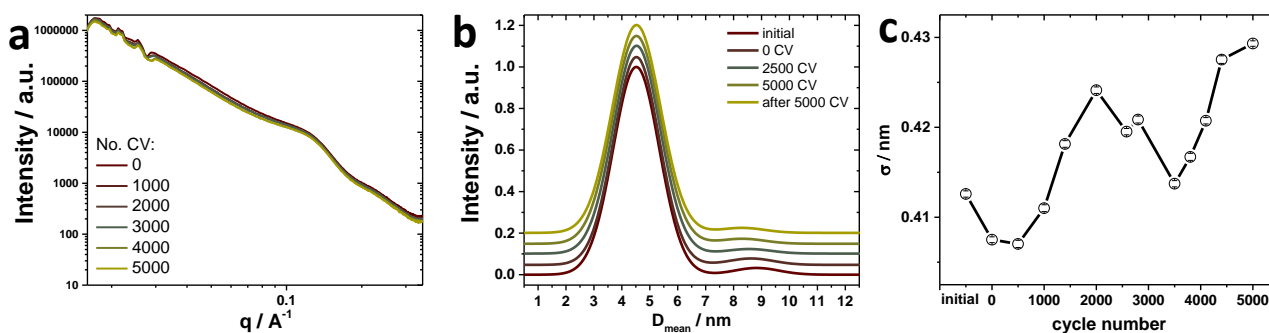


Figure S8. *In situ* ASAXS measurements for HP-AST: background subtracted, Pt element specific scattering curves for selected cycle numbers (a), particle size distribution (PSD) as a function of rel. intensity over the mean particle diameter for selected cycle numbers (b) and the evolution of polydispersity as a function of σ over the cycle number (c).

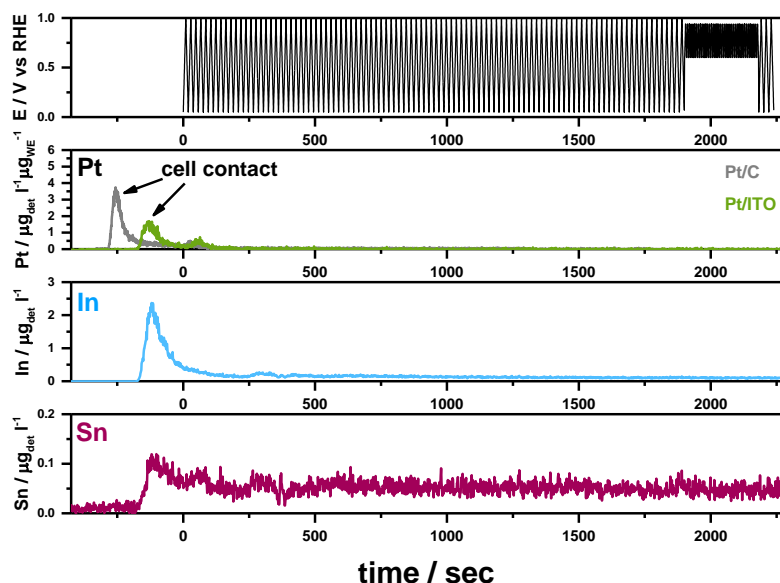


Figure S9. *In situ* scanning flow cell ICP-MS measurements. Depicted are the Sn, In and Pt dissolutions rates and the applied electrochemical protocols from the bottom to the top for LP-AST. The respective dissolution rates in detected metal per volume electrolyte ($\mu\text{g}_{\text{det}} \text{l}^{-1}$) are plotted against the time. A Pt/C reference sample was measured and therefore, the Pt dissolution rate was also normalized to the Pt mass loading on the working electrode (WE) ($\mu\text{g}_{\text{det}} \text{l}^{-1} \mu\text{g}_{\text{WE}}^{-1}$). The electrochemical protocol was conducted as follows: Beginning with 100 CVs (activation regime) from 0.05-1 V, followed by potential cycling in the LP regime (0.6-0.95 V, 40 CVs, $100 \text{ mV} \cdot \text{s}^{-1}$) and followed by another 3 cycles from 0.05-1 V, all CVs were recorded with a scan rate of 100 mV/s . The first contacts between catalyst and electrolyte (cell contact) are denoted with arrows.

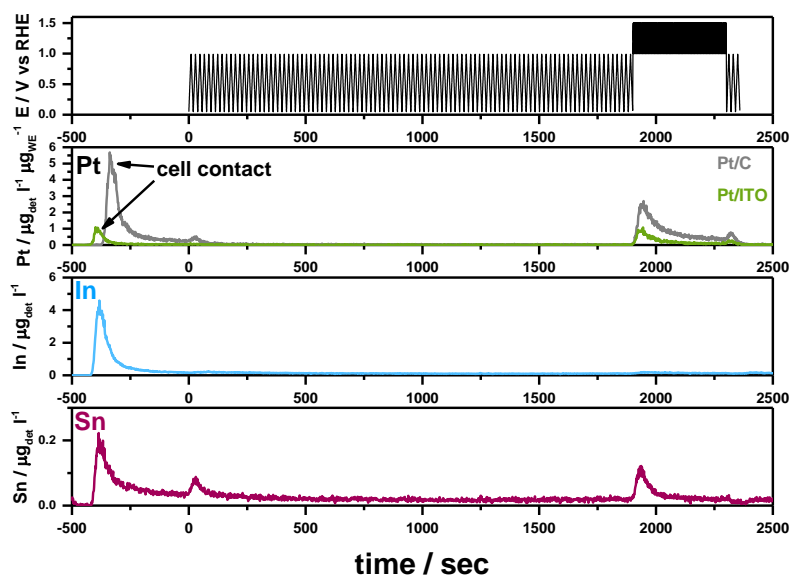


Figure S10. *In situ* scanning flow cell ICP-MS measurements. Depicted are the Sn, In and Pt dissolutions rates and the applied electrochemical protocols from the bottom to the top for HP-AST. The respective dissolution rates in detected metal per volume electrolyte ($\mu\text{g}_{\text{det}} \text{l}^{-1}$) are plotted against the time. A Pt/C reference sample was measured and therefore, the Pt dissolution rate was also normalized to the Pt mass loading on the working electrode (WE) ($\mu\text{g}_{\text{det}} \text{l}^{-1} \mu\text{g}_{\text{WE}}^{-1}$). The electrochemical protocol was conducted as follows: Beginning with 100 CVs (activation regime) from 0.05-1 V, followed by potential cycling in the HP regime (1.0-1.5 V, 200 CVs, $500 \text{ mV} \cdot \text{s}^{-1}$) and followed by another 3 cycles from 0.05-1 V, all CVs were recorded with a scan rate of 100 mV/s . The first contacts between catalyst and electrolyte (cell contact) are denoted with arrows.

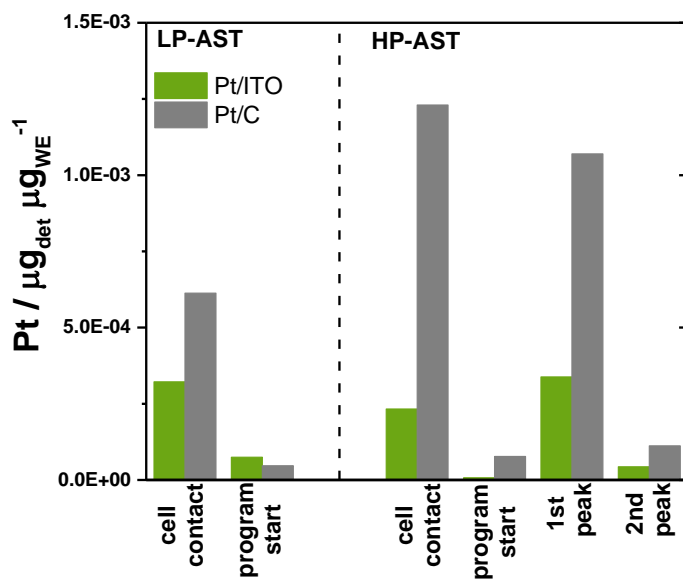


Figure S11. Results from *in situ* SFC ICP-MS of the integration of the peaks arising from Pt dissolution over time of the measurement (in μg_{det}) detected by the ICP-MS per mass loading Pt on the working electrode (in μg_{WE}) for LP- and HP-AST.

Table S3. Results from *in situ* SFC ICP-MS of the integration over time of the measured peaks arising from Pt dissolution in Pt/ITO and Pt/C reference and In and Sn from ITO support. Pt dissolution in μg is normalized to Pt mass loading on the working electrode in μg_{Pt} and In and Sn dissolution in μg is normalized to In+Sn mass loading on the working electrode in $\mu\text{g}_{(\text{In}+\text{Sn})}$. Potential dissolution peaks are arising from cell contact, program start and distinct dissolution peaks during the electrochemical cycling (1st and 2nd peak). Additionally, dissolution values are listed each without (wo/) and with (w/) contribution of metal dissolution at cell contact.

	LP-AST				HP-AST			
Dissolved Metal	Pt in Pt/ITO	Pt in Pt/C	In	Sn	Pt in Pt/ITO	Pt in Pt/C	In	Sn
Unit	$\mu\text{g} \cdot \mu\text{g}_{\text{Pt}}$		$\mu\text{g} \cdot \mu\text{g}_{(\text{In}+\text{Sn})}$		$\mu\text{g} \cdot \mu\text{g}_{\text{Pt}}$		$\mu\text{g} \cdot \mu\text{g}_{(\text{In}+\text{Sn})}$	
Cell Contact	3.22E-4	6.13E-4	5.55E-3	3.52E-4	2.33E-4	1.23E-3	1.04E-2	1.19E-3
Program Start	7.47E-5	4.66E-5	-	-	7.22E-6	7.74E-5	-	2.80E-4
1st Peak	-	-	-	-	3.38E-4	1.07E-3	-	3.00E-4
2nd Peak	-	-	-	-	4.32E-5	1.12E-4	-	-
Total wo/ Contact	5.96E-5	3.36E-4	9.61E-3	3.41E-3	7.37E-4	1.68E-3	9.12E-3	3.96E-3
Total w/ Contact	3.80E-4	9.49E-4	1.51E-2	3.77E-3	9.69E-4	2.91E-3	1.95E-2	5.15E-3
Total wo/ Contact %	0.01	0.03	0.96	0.34	0.07	0.17	0.91	0.40
Total w/ Contact %	0.04	0.09	1.51	0.38	0.10	0.29	1.95	0.52

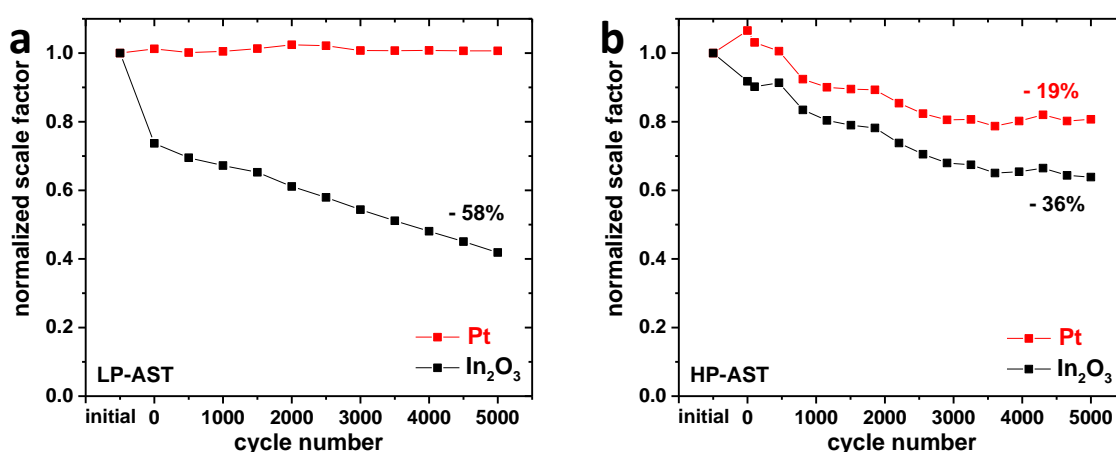


Figure S12. Evolution of normalized scale factors for Pt and In₂O₃ from fits of HE-XRD patterns over the cycle number for (a) LP-AST and (b) HP-AST.

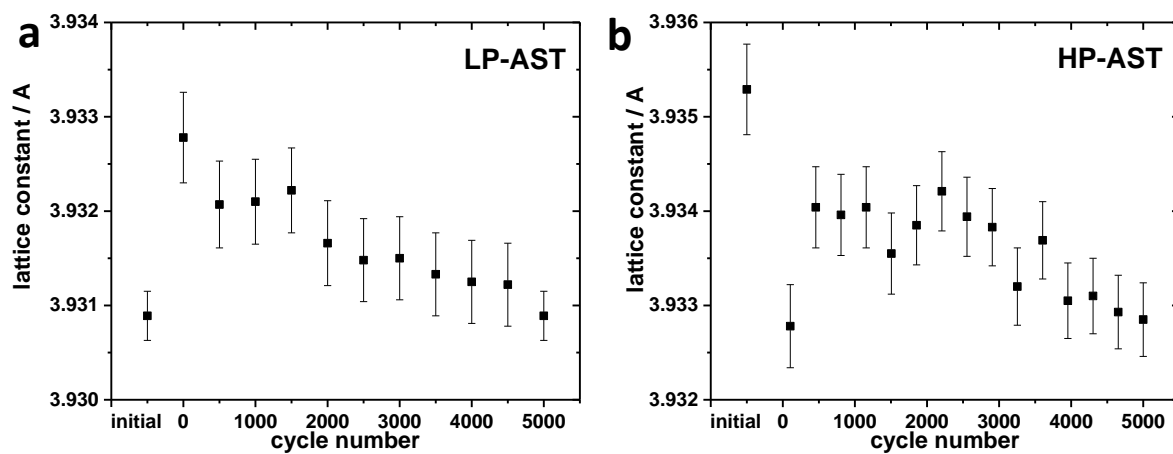


Figure S13. Evolution of Pt lattice constant as extracted from Rietveld Refinement from *in situ* HE-XRD measurements over the cycle number for (a) LP-AST and (b) HP-AST.